Available online at www.sciencedirect.com
SCIENCE DIRECT
International Journal of Heat and Mass Transfer 49 (2006) 2739–2750
International Journal of HEAT and MASS TRANSFER
www.elsevier.com/locate/ijhmt

A macroscopic turbulence model for flow in porous media suited for channel, pipe and rod bundle flows

M. Chandesris [a], G. Serre [a,*], P. Sagaut [b]

[a] Laboratoire de Modélisation et Développement Logiciels, DEN/DER/SSTH, CEA Grenoble, 17 rue des Martyrs, 38054 Grenoble Cedex 9, France
[b] Laboratoire de Modélisation en Mécanique UMPC-CNRS, 4 place Jussieu, Tour 66, Case 162, 75252 Paris Cedex 05, France

Received 23 December 2004; received in revised form 15 July 2005
Available online 9 March 2006

Abstract

In the literature, a macroscopic two-equation turbulence model is proposed for analyzing turbulent flows through porous media of particular morphologies (arrays of square or circular rods, packed spheres). This model has been adapted to longitudinal flows in channels, pipes and rod bundles, in order to be able to analyze turbulent flows within nuclear power reactor circuits and core using a macroscopic turbulence model. The additional source terms of the macroscopic k–ϵ equations, which appear as an output of the volume-averaging process, are modeled using the kinetic energy balance and physical considerations. The two unknown constants of the closure expression are determined from the spatial averaging of microscopic k–ϵ computations and from numerical and experimental results available in the literature. This present model has been first successfully evaluated in various simple geometries such as channel and pipe. Good agreement was also obtained between this present model and an experiment of decreasing turbulence inside a rod bundle.

Keywords: Turbulence modeling; Porous media; Incompressible flow; Volume-average

1. Introduction

In the core of a nuclear power reactor, complex thermo-hydraulic phenomena occur and a detailed description of the flow may be required. Time-dependent, high resolution simulations based on Large Eddy Simulation (LES) or on Reynolds Averaged Navier–Stokes (RANS) models are able to give the desired detailed flow field prediction. However, the exorbitant run time associated with such simulations and the actual limit of the calculators restrict their use to a limited region of the system. Furthermore, these simulations depend on the state of the flow in the remaining part of the system. This requires either an artificial isolation of the interesting region, or, preferably a coupling between the high resolution description on that region and another description of the remaining part of the system based on a less detailed, cheaper resolution. Macroscopic descriptions such as those developed in the porous media framework, could fulfill this need for a coarse resolution. Indeed, with a porous media formulation, all the complex geometry of the core reactor would not be described, reducing the cost of the computation, but the overall effect of the solid would be taken into account in the model. Therefore, a porous media formulation seems well adapted to the development of a turbulence model dedicated to charged medium such as those encountered in the core of a nuclear reactor. However, in order to be able to later consider the coupling between the different levels of description, the macroscopic turbulent model has to be consistent with microscopic turbulent models, and thus to be properly derived.

In the study of flow through porous media, the first works were mainly based on semi-empirical laws [8]. It is only recently that general equations for flows through porous media were formally derived using the volume-averaging technique [33]. Lage [21] gives a very interesting and comprehensive review of this history of the modeling of

* Corresponding author. Tel.: +33 4 38 78 53 59; fax: +33 4 38 78 50 36.
E-mail address: guillaume.serre@cea.fr (G. Serre).

0017-9310/$ - see front matter © 2006 Elsevier Ltd. All rights reserved.
doi:10.1016/j.ijheatmasstransfer.2005.12.013

Nomenclature

c_1, c_2, C_μ	turbulence model constants
C_f	friction coefficient
c_p, y^+_{lim}	macroscopic turbulence model constants
D_h	hydraulic diameter
k	turbulent kinetic energy
K	permeability
p	pressure
Re_H	Reynolds number
S_w	wall friction surface
u_i	velocity

Special symbols

$\langle\psi\rangle$	volume average
$\langle\psi\rangle_f$	intrinsic average
$\overline{\psi}$	ensemble mean
ψ'	fluctuation
$\delta\psi$	deviation from intrinsic average

Greek symbols

ϕ	porosity
ϵ	dissipation rate of turbulent kinetic energy
ν	kinematic viscosity
ν_t	turbulent viscosity
ν_{t_ϕ}	macroscopic turbulent viscosity
ρ	fluid density
$\tilde{\sigma}_k$, $\tilde{\sigma}_\epsilon$	macroscopic Prandtl numbers

flow through porous media starting from the work of Darcy. The volume-averaging technique is a rigorous mathematical procedure used to derive the governing mass, momentum and energy equations in porous media [3,34]. Different authors use this formalism to derive macroscopic turbulence models. For instance, Masuoka and Takatsu [23] derive a 0-equation turbulence model using the local volume-averaging technique. They model the effective eddy diffusivity as the algebraic sum of the eddy diffusivities estimated from two types of vortices: the pseudo vortex and the interstitial vortex. Studying also turbulent flow and heat transfer through stacked spheres, Alvarez et al. [1] propose a 1-equation turbulence model.

Two-equation macroscopic turbulence models are also proposed in the literature. Antohe and Lage [2] derive a two-equation macroscopic turbulence model applying the time averaging operator to the extended Darcy–Forchheimer model. Getachew et al. [13] extend this work by taking into account higher order terms. Following another approach, Nakayama and Kuwahara [25] propose a two-equation macroscopic turbulence model obtained by spatially averaging the Reynolds-averaged Navier–Stokes equations. However, for turbulent flows, the order of application of the two operators (time-averaging for turbulence and volume averaging) is important. Pedras and de Lemos [27] show that the two approaches lead to similar equations for the mean flow, but that the turbulence kinetic energies resulting from the two different approaches are different. In particular, they show that, applying first the time-averaging operator, allows to take into account the turbulence inside the pores. Thus, the latter approach will be used in our study.

Applying the volume-averaging theory to the microscopic transport equations of turbulent kinetic energy and its dissipation rate, Nakayama and Kuwahara [25], and Pedras and de Lemos [28], establish a macroscopic two-equation turbulence model. They obtain a new set of equations for the transport of the volumetric averaged turbulence kinetic energy and its dissipation rate. These new equations involve additional terms which quantify the influence of the medium morphology on the turbulent kinetic energy and dissipation level. The main difficulty of the approach is to propose a closure for these additional terms and unfortunately there is no general well-developed closure expression valid for any kind of porous media morphology for these additional terms. Nakayama and Kuwahara [25], and Pedras and de Lemos [28] propose different models for these additional terms. The important point is that the correlations, or the constant of their models are obtained by integrating microscopic results obtained from numerical experiments over a unit porous structure. Different unit porous structures have been already considered: regular morphology made of square [25], circular [30] or elliptic [29] rods. This method of integrating microscopic results obtained from numerical experiments over a unit porous structure has also been used with success by Kuwahara et al. [19,20] and Nakayama et al. [26] to study thermal dispersion and interfacial heat transfer coefficient in porous media.

We are interested in modeling the core of nuclear power reactors using the porous media approach. The different nuclear cores that are under study are characterized by elongated geometries, and by a large number of identical elements. As can be seen in Fig. 1, which shows examples of gas cooled reactors, we can have to compute the turbulent flows around more than thousands of needles, and we are interested by different geometries: channels, tubes and needles. Furthermore, in the core of the reactor, the flow is longitudinal whereas in the studies by Nakayama and Kuwahara [18,25], and Pedras and de Lemos [28–30] only transverse flows were considered. Chung et al. [6] have already studied a porous media made of channels. However, their work is based on the model of Antohe and Lage [2]. As mentioned previously, this model does not allow to take into account the turbulent kinetic energy inside the interstices, while we are precisely interested in knowing

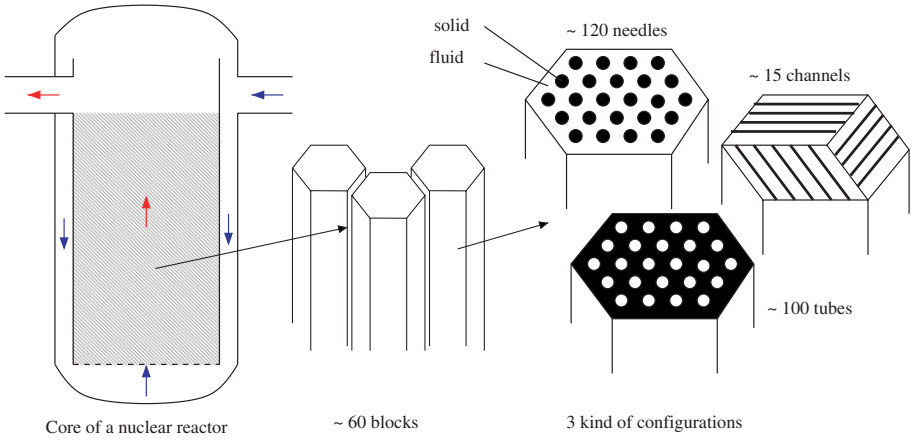

Fig. 1. Example of geometries under study for the core of a nuclear reactor.

the level of turbulence inside the channels. Thus, our purpose is twofold. First, to study the additional source terms for longitudinal flows through various geometries, using the approach proposed by Nakayama and Kuwahara [25]. Second, to take advantage of the simplicity of the studied geometries to establish the closure expressions not only by solving the microscopic flow inside periodic elementary cells, as was done for transverse flows, but also by using physical considerations.

The first part of this paper will focus on the mathematical formalism of the volume-averaging theory. Then the macroscopic equations of mass, momentum, turbulent kinetic energy and its dissipation rate obtained by applying the time-averaging operator prior to the volume-averaging operator are presented. In the second part, closure expressions for the additional source terms appearing in the macroscopic k–ϵ transport equations are obtained based on physical considerations. These closure expressions are dedicated to longitudinal flows through elongated geometries. The unknown constants of this model are established in the third part using numerical and experimental results. Finally, the macroscopic turbulence model is evaluated for unidirectional turbulent flows using two sets of data of decreasing turbulence, one numerical and the other experimental.

2. Macroscopic governing equations

2.1. The volume-averaging method for flow in porous media

The main idea of the volume-averaging theory is to apply a volume-averaging operator over a representative elementary volume (REV) to the set of equations governing the considered problem at the microscopic scale (mass, momentum, scalar transport, etc.) in order to obtain a set of equations at the macroscopic level. The choice of the size of the REV is important. The size of the REV should be sufficiently small in order to preserve as much information of the unfiltered flow field as possible in the volume-averaged flow field. On the other hand, the size of the REV should be such that $\langle\langle\psi\rangle\rangle \approx \langle\psi\rangle$, i.e. the volume-averaged flow field should present negligible variations on scales smaller than the filter length. This restriction is important, because it implies that the scale of variation of the averaged flow field is larger than the size of the REV, and gives sense to the use of the volume-averaging operator. Additional terms appear due to this averaging process and the main difficulty of the approach is to propose a closure model for these additional terms.

In the study of multiphase transport phenomena, two types of volume averages are commonly introduced [35]. The first one is the *phase average* (or volumetric average) which is defined by

$$\langle\psi\rangle = \frac{1}{V}\int_V \chi\psi\,\mathrm{d}V = \frac{1}{V}\int_{V_\mathrm{f}} \psi\,\mathrm{d}V \tag{1}$$

for any physical variable ψ, where V_f represents the volume of the fluid phase contained within the averaging volume V and χ is the phase indicator function:

$$\chi = \begin{cases} 1 & \text{in the fluid phase} \\ 0 & \text{in the solid phase} \end{cases} \tag{2}$$

However, $\langle\psi\rangle$ is not equal to ψ when the latter is a constant. Therefore a second average, the *intrinsic phase average*, is defined by:

$$\langle\psi\rangle_\mathrm{f} = \frac{1}{V_\mathrm{f}}\int_{V_\mathrm{f}} \psi\,\mathrm{d}V \tag{3}$$

which is more representative of the condition in the fluid phase. These two averages are related through the porosity ϕ by

$$\langle\psi\rangle = \phi\langle\psi\rangle_\mathrm{f}, \quad \phi = \frac{V_\mathrm{f}}{V} \tag{4}$$

Using this formalism, and neglecting the classical spatial commutation error, it is possible to derive the relations between the volumetric intrinsic average of derivatives and the derivatives of volumetric intrinsic average. These

relations are presented in different works [32,34] and are known as theorems of local volumetric average. For the case of a fixed solid, they can be written as

$$\left\langle \frac{\partial \psi}{\partial x_i} \right\rangle_{\mathrm{f}} = \frac{1}{\phi}\frac{\partial}{\partial x_i}(\phi\langle\psi\rangle_{\mathrm{f}}) + \frac{1}{V_{\mathrm{f}}}\int_{\Sigma}\psi n_i \,\mathrm{d}\Sigma \tag{5}$$

$$\left\langle \frac{\partial \psi}{\partial t} \right\rangle_{\mathrm{f}} = \frac{\partial}{\partial t}\langle\psi\rangle_{\mathrm{f}} \tag{6}$$

where Σ is the interface between the fluid and the solids, while n_i is i-th component of the unit normal vector oriented outward from the fluid.

2.2. Macroscopic continuity and momentum equations

Applying the phase average operator to the microscopic Reynolds averaged equations, and using the fact that velocity fluctuations vanish at the fluid-solid interface Σ, the following result is obtained:

$$\frac{\partial \phi\langle\bar{u}_i\rangle_{\mathrm{f}}}{\partial x_i} = 0$$

$$\begin{aligned}\phi\frac{\partial\langle\bar{u}_i\rangle_{\mathrm{f}}}{\partial t} &+ \frac{\partial}{\partial x_j}(\phi\langle\bar{u}_i\rangle_{\mathrm{f}}\langle\bar{u}_j\rangle_{\mathrm{f}}) \\ &= -\frac{1}{\rho}\frac{\partial}{\partial x_i}(\phi\langle\bar{p}\rangle_{\mathrm{f}}) + \frac{\partial}{\partial x_j}\left(\nu\left(\frac{\partial\phi\langle\bar{u}_i\rangle_{\mathrm{f}}}{\partial x_j} + \frac{\partial\phi\langle\bar{u}_j\rangle_{\mathrm{f}}}{\partial x_i}\right)\right) \\ &\quad - \frac{\partial}{\partial x_j}(\phi\langle\delta\bar{u}_i\delta\bar{u}_j\rangle_{\mathrm{f}}) + R - \frac{\partial}{\partial x_j}(\phi\langle\overline{u_i'u_j'}\rangle_{\mathrm{f}})\end{aligned} \tag{7}$$

where

$$R = \frac{1}{V}\int_{\Sigma}\left(\nu\left(\frac{\partial\bar{u}_i}{\partial x_j} + \frac{\partial\bar{u}_j}{\partial x_i}\right) - \frac{\overline{p}}{\rho}\delta_{ij}\right)\cdot n_j \,\mathrm{d}\Sigma \tag{8}$$

represents the volume average of the surface drag force due to the presence of solids. $\delta\psi$ denotes the deviation of ψ from its intrinsic average $\langle\psi\rangle_{\mathrm{f}}$ such that

$$\delta\psi = \psi - \langle\psi\rangle_{\mathrm{f}} \tag{9}$$

The closure of this system is realized through the modeling of the last three unknown terms appearing in (7). The first term can be interpreted as an inertial dispersion term and the second one as a surface drag term. The inertial effects become appreciable only for high speed flow and cause an increase in the form drag. Furthermore, these two terms have the same effect. They generate a pressure drop through frictional drag. Since, for steady, macroscopically uniform flow, Eq. (7) should reduce to the semi-empirical well-known Darcy–Forchheimer law which relates the pressure drop to the flow velocity and the square of the flow velocity, Vafai and Tien [33] modeled this two terms together using the Forchheimer-extended Darcy's law. For simple and well-known geometries (plane, pipe or rod bundle flows), considering longitudinal flows, the pressure drop due to friction is known through wall friction pressure loss correlations [9,16]. Therefore, these two terms are modeled together through a friction force F.

The last term, the macroscopic Reynolds stress tensor, is modeled following an idea proposed by Pedras and de Lemos [28]. They introduce a macroscopic turbulent viscosity ν_{t_ϕ} which verify

$$\nu_{\mathrm{t}_\phi}\langle s_{ij}\rangle = \langle\nu_{\mathrm{t}} s_{ij}\rangle \tag{10}$$

where

$$s_{ij} = \frac{1}{2}\left(\frac{\partial\bar{u}_i}{\partial x_j} + \frac{\partial\bar{u}_j}{\partial x_i}\right) \tag{11}$$

Since $\bar{u}$ vanishes at the wall surface, it comes

$$\langle s_{ij}\rangle = \frac{1}{2}\left(\frac{\partial\phi\langle\bar{u}_i\rangle_{\mathrm{f}}}{\partial x_j} + \frac{\partial\phi\langle\bar{u}_j\rangle_{\mathrm{f}}}{\partial x_i}\right) \tag{12}$$

and the macroscopic Reynolds stress tensor is given by

$$-\phi\langle\overline{u_i'u_j'}\rangle_{\mathrm{f}} = 2\phi\langle\nu_{\mathrm{t}} s_{ij}\rangle_{\mathrm{f}} - \frac{2}{3}\phi\langle k\rangle_{\mathrm{f}}\delta_{ij} = 2\nu_{\mathrm{t}_\phi}\langle s_{ij}\rangle - \frac{2}{3}\phi\langle k\rangle_{\mathrm{f}}\delta_{ij} \tag{13}$$

Thus, the macroscopic momentum equation can be written as follow:

$$\begin{aligned}\phi\frac{\partial\langle\bar{u}_i\rangle_{\mathrm{f}}}{\partial t} &+ \frac{\partial}{\partial x_j}(\phi\langle\bar{u}_i\rangle_{\mathrm{f}}\langle\bar{u}_j\rangle_{\mathrm{f}}) \\ &= -\frac{1}{\rho}\frac{\partial}{\partial x_i}\left(\phi\langle\bar{p}\rangle_{\mathrm{f}} + \frac{2}{3}\phi\rho\langle k\rangle_{\mathrm{f}}\right) \\ &\quad + \frac{\partial}{\partial x_j}\left((\nu + \nu_{\mathrm{t}_\phi})\left(\frac{\partial\phi\langle\bar{u}_i\rangle_{\mathrm{f}}}{\partial x_j} + \frac{\partial\phi\langle\bar{u}_j\rangle_{\mathrm{f}}}{\partial x_i}\right)\right) + \phi F_i\end{aligned} \tag{14}$$

A method has to be proposed to compute ν_{t_ϕ}. Both Nakayama and Kuwahara [25], and Pedras and de Lemos [28] use the expression

$$\nu_{\mathrm{t}_\phi} = C_\mu\frac{\langle k\rangle_{\mathrm{f}}^2}{\langle\epsilon\rangle_{\mathrm{f}}} \tag{15}$$

which is a very simple expression inspired by the modeling at the microscopic scale. This choice will be discussed later.

2.3. Macroscopic transport equations for k and ϵ

In their work, Nakayama and Kuwahara [25] obtained the macroscopic transport equations for $\langle k\rangle_{\mathrm{f}}$ and $\langle\epsilon\rangle_{\mathrm{f}}$ by applying the intrinsic average operator to the classical two equations k–ϵ turbulent model using the modeling constants recommended by Launder and Spalding [22]. Another approach was followed by Pedras and de Lemos [28], who worked on the transport equations for k and ϵ without introducing a priori any microscopic turbulence model. Comparing their results, one can see that their macroscopic transport equations for $\langle k\rangle_{\mathrm{f}}$ and $\langle\epsilon\rangle_{\mathrm{f}}$ are very similar, except for the modeling of the additional source terms and considering that the turbulent viscosity of Nakayama and Kuwahara's model is a macroscopic turbulent viscosity. Noting P_k and S_ϵ the additional source terms, the set of transport equations for $\langle k\rangle_{\mathrm{f}}$ and $\langle\epsilon\rangle_{\mathrm{f}}$ is

Table 1
Source terms for the macroscopic turbulence models

	S_k	S_ϵ	
Nakayama and Kuwahara [25]	ϵ_∞	$c_2\frac{\epsilon_\infty^2}{k_\infty}$	$\epsilon_\infty = 39\phi^2(1-\phi)^{5/2}\frac{\langle\bar{u}\rangle_f^3}{D}$ $k_\infty = 3.7(1-\phi)\phi^{3/2}\langle\bar{u}\rangle_f^2$
Pedras and de Lemos [28]	$c_k\frac{\langle k\rangle_f\langle\bar{u}\rangle}{\sqrt{K}}$	$c_2 c_k\frac{\langle\epsilon\rangle_f\langle\bar{u}\rangle}{\sqrt{K}}$	$K = \frac{\phi^3 D^2}{144(1-\phi)^2}$ $c_k = 0.28$

$$\phi\frac{\partial\langle k\rangle_f}{\partial t} + \frac{\partial}{\partial x_j}\left(\phi\langle\bar{u}_j\rangle_f\langle k\rangle_f\right) = 2\phi\nu_{t_\phi}\langle s_{ij}\rangle_f\langle s_{ij}\rangle_f + \frac{\partial}{\partial x_j}\left(\left(\nu + \frac{\nu_{t_\phi}}{\tilde{\sigma}_k}\right)\frac{\partial\phi\langle k\rangle_f}{\partial x_j}\right) - \phi\langle\epsilon\rangle_f + \phi P_k \tag{16}$$

$$\phi\frac{\partial\langle\epsilon\rangle_f}{\partial t} + \frac{\partial}{\partial x_j}\left(\phi\langle\bar{u}_j\rangle_f\langle\epsilon\rangle_f\right) = \frac{\partial}{\partial x_j}\left(\left(\nu + \frac{\nu_{t_\phi}}{\tilde{\sigma}_\epsilon}\right)\frac{\partial\phi\langle\epsilon\rangle_f}{\partial x_j}\right) + \phi\left(2c_1\nu_{t_\phi}\langle s_{ij}\rangle_f\langle s_{ij}\rangle_f - c_2\langle\epsilon\rangle_f\right)\frac{\langle\epsilon\rangle_f}{\langle k\rangle_f} + \phi S_\epsilon \tag{17}$$

where (c_1, c_2) are the two constants of the microscopic k–ϵ model, and $(\tilde{\sigma}_k, \tilde{\sigma}_\epsilon)$ are macroscopic turbulent Prandtl numbers. These macroscopic turbulence model equations present two extra source terms P_k and S_ϵ which represent 'internal' production of turbulence kinetic energy and its dissipation rate due to the presence of solids and for which a closure model has to be proposed. The turbulence source terms models of Nakayama and Kuwahara [25] and Pedras and de Lemos [28] are summarized in Table 1.

3. The closure problem

To close the model, the easiest way is to consider the equilibrium for which it is possible to evaluate the unknown source terms (Eqs. (16) and (17)) and to deduce correlations. Here, the flow is said to be at equilibrium when the flow is steady and spatially uniform from the macroscopic point of view ($D\langle k\rangle_f/Dt = D\langle\epsilon\rangle_f/Dt = 0$), and when the turbulence is fully developed. However, it does not give the expression of the unknown source terms out of equilibrium. Then, two different ways can be followed:

- The general expression proposed to model the unknown source terms has to reduce to an expression at least valid at equilibrium. This is the point of view adopted by Pedras and de Lemos [28]. According to them, the extra source terms are linked to the current level of turbulence of the considered flow (see Table 1).
- The correlations obtained at equilibrium are valid out of equilibrium without generalizing their expressions. This is the point of view adopted by Nakayama and Kuwahara [25].

The second point of view was chosen because we have more physical arguments to explain the expression of the production terms at equilibrium, and they are unfortunately not directly transposable out of equilibrium.

3.1. Theoretical approach for longitudinal flows

The two internal source terms directly depend on the medium morphology. One can easily imagine that the turbulent kinetic energy production of a porous medium made of spheres is not the same as the one for straight parallel channels or pipes. This is why we do not use the closure expressions currently available. They are designed for transverse flows in array of square (or circular) rods, or packing of spheres and we are interested in longitudinal flows in geometries made of channels, pipes or needles as illustrated in Fig. 1.

3.1.1. Production of turbulent kinetic energy: P_k

For fully developed, uniform, uni-dimensional flows Eq. (16) reduces to

$$P_k = \langle\epsilon\rangle_f = \epsilon_\infty \tag{18}$$

ϵ_∞ being the value reached by $\langle\epsilon\rangle_f$ at equilibrium. As expected, the 'internal' production of turbulent kinetic energy P_k is balanced by the dissipation since the flow is at equilibrium and since there is no macroscopic production of turbulence. The internal production term P_k is evaluated writing the total kinetic energy balance. For fully developed, uniform, uni-dimensional flows, all the kinetic energy lost by the mean flow turns partly into heat (direct viscous dissipation), partly into turbulence through the production term that has to be evaluated

$$-\frac{1}{\rho}\frac{\partial\overline{p}}{\partial x_j}\bar{u}_j = \nu\left(\frac{\partial\bar{u}_i}{\partial x_j}\right)^2 - \overline{u_i'u_j'}\frac{\partial\bar{u}_i}{\partial x_j} \tag{19}$$

The kinetic energy balance is integrated over a control volume. For arrays of channels (or pipes), the REV includes the section of one channel (or one pipe). For the needles, the REV consist of one elementary cell as depicted in Fig. 2. The relation between the pressure gradient and the friction force is used to obtain

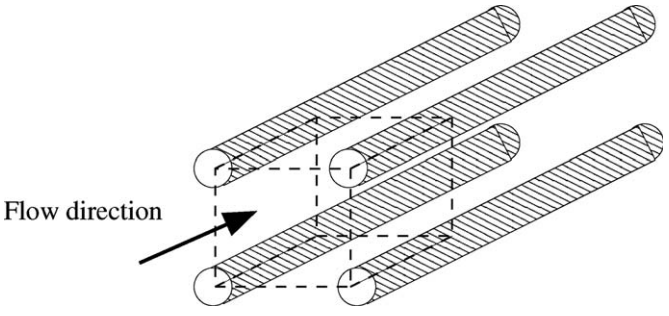

Fig. 2. REV for the array of needles.

$$\frac{1}{\rho}F_j\langle\bar{u}_j\rangle_{\mathrm{f}} = \frac{\nu}{V_{\mathrm{f}}}\int_{V_{\mathrm{f}}}\left(\frac{\partial\bar{u}_i}{\partial x_j}\right)^2 \mathrm{d}V \underbrace{-\left\langle\overline{u_i'u_j'}\frac{\partial\bar{u}_i}{\partial x_j}\right\rangle_{\mathrm{f}}}_{P_k} \tag{20}$$

where the friction force F is nonzero only in the mean flow direction, and can be related to the macroscopic velocity through a friction coefficient C_{f}

$$F = \frac{1}{2}\rho\langle\bar{u}\rangle_{\mathrm{f}}^2\frac{4C_{\mathrm{f}}}{D_{\mathrm{h}}} \tag{21}$$

D_{h} is the hydraulic diameter and can be defined for longitudinal flows by

$$D_{\mathrm{h}} = 4\frac{V_{\mathrm{f}}}{S_{\mathrm{w}}} \tag{22}$$

where S_{w} is the wall friction surface. Since most of the viscous dissipation occurs very close to the wall for longitudinal flows, i.e. where mean velocity gradients are very important, the kinetic energy transferred to heat is estimated by integrating the expression for the dissipation only in the viscous region. The mean velocity profile is known in this region and is given by the linear law $U^+ = y^+$. U^+ stands for the velocity reduced by u_τ, u_τ being the friction velocity, and y^+ is the normal coordinate expressed in wall units. Since the thickness of the viscous layer is very small at high Reynolds number compared to the other dimension of the integration domain, the volume of the viscous region is well estimated by taking the product of the thickness of the viscous layer by the wall friction surface. It comes

$$\frac{\nu}{V_{\mathrm{f}}}\int_{V_{\mathrm{f}}}\left(\frac{\partial\bar{u}_i}{\partial x_j}\right)^2 \mathrm{d}V \approx \frac{\nu}{V_{\mathrm{f}}}S_{\mathrm{w}}\int_0^{\frac{\nu}{u_\tau}y^+_{\mathrm{lim}}}\frac{u_\tau^4}{\nu^2}\,\mathrm{d}y \approx \frac{4}{D_{\mathrm{h}}}y^+_{\mathrm{lim}}u_\tau^3 \tag{23}$$

This expression is valid for longitudinal geometries with a constant section. y^+_{lim} corresponds to the limit of the integration zone expressed in wall units. Its value should be equal to the thickness of the viscous region. This limit is located somewhere in the buffer layer ($5 \leqslant y^+_{\mathrm{lim}} \leqslant 30$). The overestimation of the dissipation in the buffer layer, due to the use of the linear law, should be approximately compensated by the fact that the dissipation is neglected beyond the limit given by y^+_{lim}. For fully developed longitudinal flows, the friction velocity is related to the macroscopic velocity through the friction coefficient C_{f}:

$$u_\tau = \sqrt{\frac{C_{\mathrm{f}}}{2}}\langle\bar{u}\rangle_{\mathrm{f}} \tag{24}$$

Finally, using Eqs. (20), (21), (23) and (24), the following model is obtained for P_k

$$P_k = 2C_{\mathrm{f}}\frac{\langle\bar{u}\rangle_{\mathrm{f}}^3}{D_{\mathrm{h}}}\left(1 - y^+_{\mathrm{lim}}\sqrt{\frac{C_{\mathrm{f}}}{2}}\right) \tag{25}$$

The production of turbulent kinetic energy is directly linked to the power of the friction forces on the walls. However, this power is corrected by the direct dissipation of kinetic energy into heat, term that is often neglected in the literature. The geometry is taken into account only through the friction coefficient C_{f}.

3.1.2. Production of dissipation: S_ϵ

The equation for $\langle\epsilon\rangle_{\mathrm{f}}$ (17) does not contain any explicit production term of dissipation (except for the macroscopic production term of dissipation $(2c_1\nu_{\mathrm{t}_\phi}\langle s_{ij}\rangle_{\mathrm{f}}\langle s_{ij}\rangle_{\mathrm{f}}\langle\epsilon\rangle_{\mathrm{f}}/\langle k\rangle_{\mathrm{f}})$ which is zero for macroscopic uniform flows with zero mean shear), whereas it should. Thus S_ϵ has to represent at least a production term of dissipation. However, it does not mean that this term represents only production. But, since no information on other phenomena is available, the assumption is made that S_ϵ represents only the net production of dissipation inside the integration domain.

To model this production of dissipation, we go back to the ideas used to derived the standard k–ϵ model. The production of dissipation should be proportional to the kinetic energy production. This idea comes from the fact that the dissipation rate is also the spectral flux of energy (cascade from the largest to the smallest eddies), and depends on the energy contained in the largest scales, which is directly linked to the production of kinetic energy. The production of dissipation should involve a production time scale. Indeed, the original dissipation equation for homogeneous flow is classically interpreted as a time scale balance:

$$\frac{1}{\epsilon}\frac{\mathrm{d}\epsilon}{\mathrm{d}t} = c_1\frac{P}{k} - c_2\frac{\epsilon}{k} \tag{26}$$

$$\frac{1}{\tau_\epsilon} \approx \frac{1}{\tau_{\mathrm{p}}} - \frac{1}{\tau_k} \tag{27}$$

The time scale of dissipation τ_ϵ is balanced by the production time scale τ_{p} and the decay time scale τ_k. Finally, the source term has to be coherent with the equilibrium state. The simplest solution that verifies these three conditions is

$$S_\epsilon = c_2\frac{P_k}{\tau_{\mathrm{p}}} \tag{28}$$

Several time scales can be proposed for τ_{p}:

1. The decay time scale:

$$\tau_{\mathrm{p}} = \frac{\langle k\rangle_{\mathrm{f}}}{\langle\epsilon\rangle_{\mathrm{f}}} \tag{29}$$

It leads to an expression similar to the traditional form of the k–ϵ model. However, this solution constrains too much the system, and does not allow to separate the effects of production and destruction.

2. A production time scale:

$$\tau_{\mathrm{p}} = \frac{\langle k\rangle_{\mathrm{f}}}{P_k} \tag{30}$$

This time scale was introduced by Chen and Kim [5] in the dissipation equation of the k–ϵ model in order to improve the standard model. This is this time scale that Nakayama and Kuwahara [25] have indirectly chosen, with the value of $\langle k\rangle_{\mathrm{f}}$ at equilibrium (noted k_∞).

We chose to use this time scale (30) since Nakayama and Kuwahara obtained good results for their geometries. It comes

$$S_\epsilon = c_2 \frac{P_k^2}{k_\infty} \tag{31}$$

A model has been already proposed for P_k (Eq. (25)). However, a model has to be proposed for k_∞. Furthermore, this small development shows how to propose a model for the production of dissipation and can be used to propose models where other phenomena have to be taken into account (singularities due to spacer grids, two-phase flows, etc.).

For fully developed, uniform, uni-dimensional flows, using Eq. (31), the transport equation of dissipation (17) reduces to

$$\langle k \rangle_f = k_\infty \tag{32}$$

k_∞ is evaluated using the classical local relation for fully developed turbulence:

$$\epsilon = \frac{k^{3/2}}{L} \tag{33}$$

where L is a characteristic turbulence length scale. This relation, often used at the microscopic level, is not directly transposable to the macroscopic level since the average of a product is not equal to the product of the averages. However, we make the hypothesis that this relation still holds at the macroscopic level using the ad hoc length scale which naturally appears in Eq. (25):

$$\epsilon_\infty = \frac{k_\infty^{3/2}}{L_M}, \quad L_M \propto \frac{D_h}{1 - y_{lim}^+ \sqrt{\frac{C_f}{2}}} \tag{34}$$

Using relations (18), (25) and (34), it comes

$$k_\infty = c \langle \bar{u} \rangle_f^2 C_f^{2/3} \tag{35}$$

This relation gives an estimation of the average level of turbulent kinetic energy when the turbulence is developed, knowing the bulk velocity and the friction coefficient. Using the Reynolds dependency at the power $-1/4$ of the friction coefficient for pipe and channel flows [9,16] this relation can also be written in the following form:

$$k_\infty = c_p \langle \bar{u} \rangle_f^2 Re_H^{-1/6} \tag{36}$$

where Re_H is the Reynolds number based on the hydraulic diameter and the bulk velocity, c_p is a constant that has to be evaluated. We could also evaluate the constant c. However it is equivalent since for most geometries empirical relations link the friction coefficient and the Reynolds number.

4. Determination of the model constants

Two constants remain unknown in our model: c_p and y_{lim}^+. They are established by integrating microscopic results obtained from experiments and numerical computations for fully developed, uniform pipe and channel flows, i.e. when relations (18) and (32) hold. Having the microscopic turbulence fields, the intrinsic volume averaged values are obtained by integrating the microscopic turbulent quantities over the fluid phase in a section of the pipe or channel (the turbulent quantities do not depend on the mean flow direction).

4.1. Numerical procedure

All the computations of that study are carried out using the TRIO_U code [4] developed at CEA (French Atomic Agency). This object oriented software is dedicated to the simulation of thermal-hydraulics problems encountered in the nuclear industry. It is able to deal with both LES and RANS models. The numerical model is based on a finite volume method which can be applied either to structured or unstructured grids. The discrete form of the equations is solved using a matrix projection scheme which is a sequel of the SOLA method originally developed by Hirt [15] (more details about this projection method can be found in Ref. [11]). In our study, calculations were carried out on a structured and staggered Cartesian grid: scalar quantities are estimated at the center of cells and velocity components at the center of cell faces. Time integration and spatial discretization schemes were common to all computations. Time advancement was ensured by a 3rd order Runge–Kutta explicit scheme. We used a centered scheme for convection and diffusion terms in the momentum equation, and an upwind scheme for the convection in the transport equations of k and ϵ.

The microscopic calculation domain considered here, is either one channel or one pipe. For the channel, the model reduces to a two-dimensional model, since the considered quantities do not depend on the spanwise direction. For the pipe, the microscopic set of governing equations reduces to a two-dimensional axisymmetric problem, using the axial symmetry around the cylinder's axis. On the solid walls, wall functions are applied in order to avoid the cost of a mesh refinement. The first computational node is located in the logarithmic zone ($y^+ > 30$) of the velocity profile where

$$U^+ = \frac{1}{\kappa} \ln(y^+) + A \tag{37}$$

κ is the Von Karman constant ($\kappa = 0.415$) and A is another constant equal to 5.32 in our study. Furthermore, in the logarithmic region, the equilibrium assumption between production and dissipation leads to the following estimations for k and ϵ:

$$k = \frac{u_\tau^2}{\sqrt{C_\mu}}, \quad \epsilon = \frac{u_\tau^3}{\kappa y} \tag{38}$$

These relations are used to compute the values of k and ϵ at the first node. In order to obtain fully developed, uniform flows, periodic conditions are applied at the ongoing-outgoing boundaries. Calculations are carried out for a wide

range of Reynolds number Re_H: $[2,5\cdot 10^4 - 5.10^5]$ for the channel, $[5\cdot 10^4 - 10^6]$ for the pipe. For each computation, the grid size in the normal direction is chosen such that the first velocity node is at a distance $y^+ = 40$ from the wall, so that the use of the wall function is valid. The largest mesh is obtained for the largest Re_H: 100×440 nodes. It has been verified that the results were grid-independent, and that the microscopic pressure gradients obtained, agreed well with the existing correlations for channel and pipe flows.

4.2. Results from microscopic model

For the channel, the results obtained from the DNS of Moser et al. [24], the experimental results obtained by Comte-Bellot [7] and our own numerical results obtained with the standard k–ϵ model are integrated over the channel section to obtain the values of k_∞ and $\epsilon_\infty = P_k$. Then c_p and $y^+_{\lim}$ can be computed:

$$c_p = \frac{k_\infty}{\langle\bar{u}\rangle_f^2} Re_H^{1/6}, \quad y^+_{\lim} = \left(1 - \frac{P_k D_h}{2C_f\langle\bar{u}\rangle_f^3}\right)\sqrt{\frac{2}{C_f}} \tag{39}$$

The results are presented in Fig. 3. We could not compute the values of $y^+_{\lim}$ of Comte-Bellot's experiment, since we only had access to the turbulent kinetic energy, and not to its dissipation rate.

For the pipe, the results of the DNS of Eggels et al. [10], the experimental results of Perry et al. [31] and also our own numerical results obtained with the standard k–ϵ model are integrated. The results for c_p and $y^+_{\lim}$ are presented in Fig. 4. Here again, we cannot present the values of $y^+_{\lim}$ for the DNS and the experiment, since the results for the dissipation rate are not available.

Fig. 3(a) and Fig. 4(a) show that the value of c_p does not depend on the Reynolds number for both geometries. This result imply that k_∞ does depend on the Reynolds number, which is a result different from the one obtain by Nakayama et al. (see Table 1). This can be explained by the fact that the studied topologies are of very different kind. Contrary to longitudinal flows in channels or pipes, transverse flows in array of rods present form drag. These figures also show a dependency of c_p on the geometry. Fig. 3(b) and Fig. 4(b) show that the values of $y^+_{\lim}$ do not depend too much on the Reynolds number, even though we observe that $y^+_{\lim}$ decrease slightly with Re_H. Furthermore, as predicted in Section 3, $y^+_{\lim}$ belongs to the buffer layer. These figures comfort the validity of our theoretical developments and suggest the following values for the two constants:

$$\text{channel:}\quad c_p = 0.0306, \quad y^+_{\lim} = 8 \tag{40}$$

$$\text{pipe:}\quad c_p = 0.0367, \quad y^+_{\lim} = 7 \tag{41}$$

One could argue that the dependency of c_p on the geometry, even for very similar geometries is a failure of the model. However, the aim was to understand the form of the correlations, result that was achieved and we recall that even the correlations for pressure head loss are different for pipes and channels:

$$\text{channel:}\quad \lambda = 0.292 Re^{-1/4} \quad \text{(Dean correlation)} \tag{42}$$

$$\text{pipe:}\quad \lambda = 0.3164 Re^{-1/4} \quad \text{(Blasius correlation)} \tag{43}$$

These results, obtained in channels and pipes, are also compared with results obtained by Pedras et al. [28] for arrays of circular rods. To draw a comparison, we compute their constant c_k which only depends on the state of the flow when it is uniform and fully-developed, and is given in their geometry by

$$c_k = \frac{\epsilon_\infty\sqrt{K}}{k_\infty\langle\bar{u}\rangle} \tag{44}$$

where K is the permeability of the porous media. c_k is the ratio between two time scales: a convective time scale (T_c) associated to the porous media, $\sqrt{K}/\langle\bar{u}\rangle$ and the turbulent time scale (T_t) associated to the internal production of turbulent kinetic energy introduced in Section 2.3: k_∞/P_k ($= k_\infty/\epsilon_\infty$ at equilibrium). For one channel (or one pipe) the permeability is obtained from the head loss for laminar flows: $K = D_h^2/48$ for the channel (respectively $K = D_h^2/32$ for the pipe). For arrays of channels or pipes the permeability depends on the porosity: $K = \phi D_h^2/48$ for channels (respectively $K = \phi D_h^2/32$ for pipes). The length given by $\sqrt{K}$ behave as $\sqrt{\phi}D_h$. With the same interstice length (D_h), you can have different permeabilities. $\sqrt{K}$ is not any more the most appropriate length scale to describe the

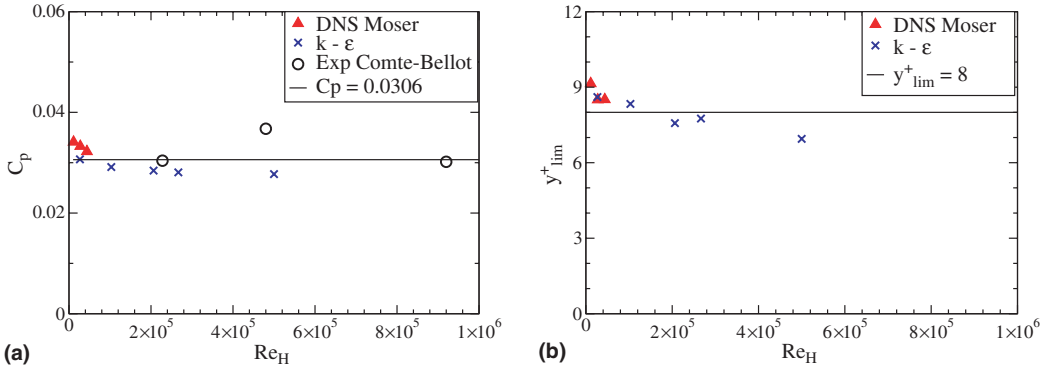

Fig. 3. Effect of Reynolds number on the two constants for the channel: (a) determination of c_p and (b) determination of $y^+_{\lim}$.

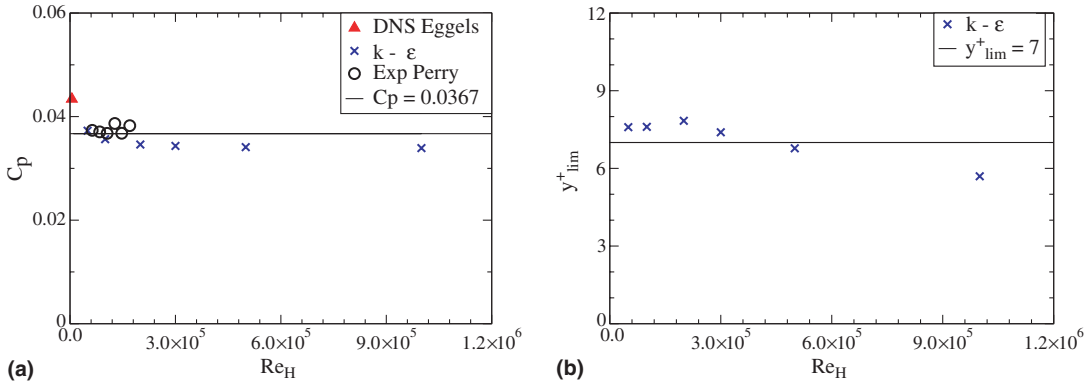

Fig. 4. Effect of Reynolds number on the two constants for the pipe: (a) determination of c_p and (b) determination of y^+_{lim}.

length of the pores, as it was for transverse flows. Thus, for longitudinal flows, c_k is redefined using the hydraulic diameter, which is a more appropriate length scale to describe the length of the interstices

$$c_k = \frac{\epsilon_\infty D_\text{h}}{k_\infty \langle \bar{u} \rangle_\text{f} 4} \tag{45}$$

As can be seen in Fig. 5(a), the order of magnitude for c_k is the same as the one found by Pedras et al. [28]. However, for our geometries, c_k shows a slight dependence on the Reynolds number and on the geometry. This dependence is also seen when computing c_k using relations (25) and (35)

$$c_k = \frac{C_\text{f}^{1/3}}{2c_p}\left(1 - y^+_{\text{lim}}\sqrt{\frac{C_\text{f}}{2}}\right) \tag{46}$$

Since C_f is a function of the Reynolds number, we recover the dependency of c_k on the Reynolds number. The constant c_k is also computed based on the correlations obtained by Nakayama et al. [25] for arrays of square rods

$$c_k = 0.878\phi\sqrt{1-\phi} \tag{47}$$

Fig. 5(b) shows the comparison. The order of magnitude for the values of c_k is still the same. However, the values of c_k obtained by Nakayama et al. do depend on the porosity.

The order of magnitude of c_k is the same for these four different geometries (pipe, channel, arrays of square and circular rods). Indeed, at equilibrium, the ratio of the convective time scale to turbulent time scale is situated in a narrow range of values: [0.16–0.34] (see Table 2). An interpretation could be:

Assuming the validity, at first order, of the equilibrium relation between averaged turbulent quantities:

$$\epsilon_\infty \sim \frac{k_\infty^{3/2}}{l} \tag{48}$$

l being the energy carrying eddies length scale, c_k can be expressed as follow:

$$c_k = \frac{T_\text{c}}{T_\text{t}} \sim \frac{\sqrt{K}}{\langle \bar{u} \rangle}\frac{\sqrt{k_\infty}}{l} \tag{49}$$

Table 2
Expression and range of values of c_k for different geometries

Geometry	Analytical expression	Range of values
Arrays of circular rods [28]	0.28	0.28
Arrays of square rods [25]	$0.878\phi\sqrt{1-\phi}$	[0.16–0.34]
Channel and pipe (present results)	$\frac{C_\text{f}^{1/3}}{2c_p}\left(1 - y^+_{\text{lim}}\sqrt{\frac{C_\text{f}}{2}}\right)$	[0.22–0.34]

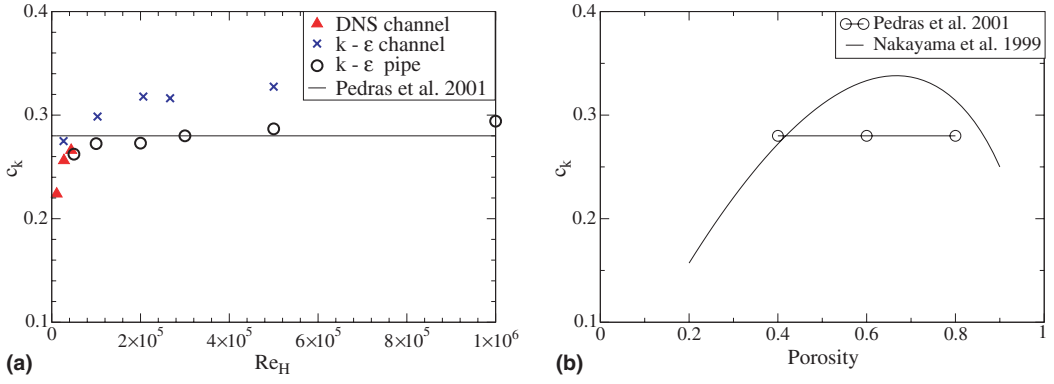

Fig. 5. Comparison for c_k: (a) c_k versus Re_H and (b) c_k versus the porosity.

Admitting that the energy carrying eddies length scale is limited by the characteristic porous length scale ($\sqrt{K} \sim l$), it comes

$$c_k \sim \frac{\sqrt{k_\infty}}{\langle \bar{u} \rangle} \sim I \tag{50}$$

I being the turbulent intensity. Thus, the average of the turbulent intensity over a porous unit structure shows a very little dependence on the topology of the porous media. This result can be observed thanks to the use of the intrinsic average operator.

In spite of this result, we do not use the correlations proposed by Pedras and de Lemos [28] for different reasons. First, even if the order of magnitude of c_k is constant, c_k does vary for our geometries and we are interested in computing as accurately as possible the mean level of turbulent kinetic energy. Secondly, the closure expressions proposed by Pedras and de Lemos [28] are directly linked to turbulent quantities (see Table 1). This choice leads to an overestimation of the dissipation of turbulent kinetic energy as can be seen on their figure 5 [28]. Furthermore, Guo et al. [14] also find out that the model proposed by Nakayama and Kuwahara [25] is the best in predicting a reasonable eddy diffusivity for gas flow in a packed bed. However, we acknowledge that a strong hypothesis is done when considering that the extra source terms are only linked to the state of the flow when it is at equilibrium.

When solving the closure problem, we showed that the production of turbulent kinetic energy is directly linked to the power of the friction forces corrected by the direct dissipation of kinetic energy into heat. Since this last term is often neglected in the literature, we present in Fig. 6 the percentage of the energy which is directly dissipated η, and which is given by

$$\eta = 1 - \frac{P_k}{2C_f \frac{\langle \bar{u} \rangle_f^3}{D_h}} \tag{51}$$

As can be seen on this figure, this percentage decrease with the Reynolds number and is clearly not negligible.

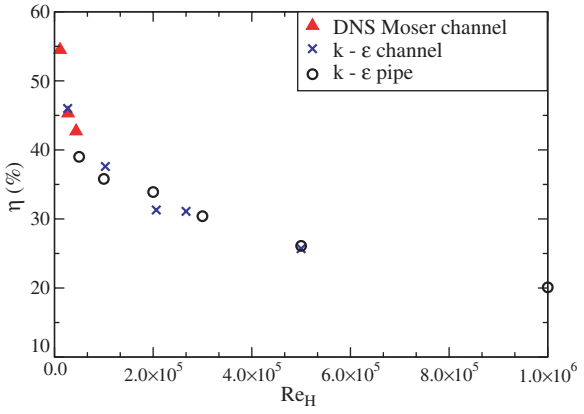

Fig. 6. Relative importance of the direct dissipation term.

5. Assessment of the macroscopic model

5.1. Channel flow

In order to assess the macroscopic turbulence model, we study first the decay of turbulence inside a channel of length $5D_h$ at $Re_H = 10^5$, from both microscopic and macroscopic points of view. This problem is two-dimensional, since there is no dependency in the spanwise direction. At the microscopic scale, the flow is computed using the standard k–ϵ model. Then the microscopic results for turbulence quantities are integrated over the section of the channel, to obtain the decay of turbulence. The grid size in the normal direction is still chosen such that the first velocity node is at a distance $y^+ = 40$ from the wall (we use wall functions on the solid walls). The size of the mesh is quite small for that Reynolds number: 100×62. At the macroscopic scale, the macroscopic turbulence model equations proposed here are solved. Symmetry conditions are used for the upper and lower boundaries, since the averaging of the no-slip condition at the wall leads to a symmetry condition. In the normal direction, only one node is taken, since the problem reduces to a one-dimensional problem, and in the streamwise direction, we set

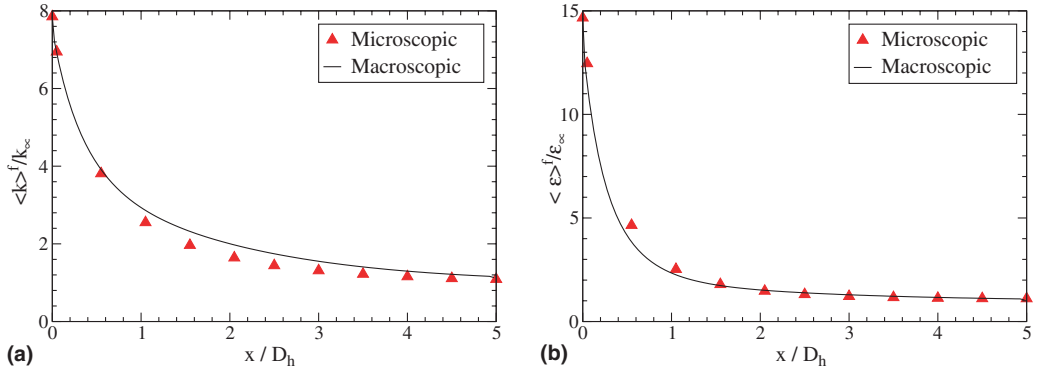

Fig. 7. Decay of turbulence: (a) turbulent kinetic energy and (b) dissipation rate of turbulent kinetic energy.

$\Delta x = D_h/20$ to have a sufficient resolution for the first points, however, it is possible to consider larger Δx. For both calculations, the inlet turbulence kinetic energy and its dissipation rate are set to $\langle k\rangle_f = 8k_\infty$ and $\langle \epsilon\rangle_f = 15\epsilon_\infty$. In both macroscopic and microscopic computations, the grid-independence of the solutions was checked. Fig. 7(a) and (b) shows the decay predicted by the present macroscopic model along with the intrinsically averaged values obtained with the microscopic computation. Good agreement between the two sets of results gives support to the present model. In particular, the use of correlations obtained at equilibrium, out of equilibrium seems to be valid since a good prediction of the decay of turbulence is obtained.

5.2. Bundle of rods (AGATE)

We also compare our model with the results of a decaying turbulence experiment *AGATE* [12] at $Re_H = 8.7 \times 10^4$. The experiment consists of a bundle of 25 rods (5×5) inside a cylinder of square section with a spacer grid at the entrance (Fig. 8). The grid generates turbulence at the entrance. Behind the grid the turbulence decays and reaches an asymptotic nonnull value due to the turbulence production by the rods. The main flow is longitudinal. The velocities and their fluctuations are measured in the section at several locations downstream the grid. The microscopic results of turbulence quantities are integrated over the fluid section to obtain the level of turbulence. The experiment only gives access to the values of the turbulent kinetic energy, and not to the dissipation rate.

Then, we look at the experiment from a macroscopic point of view. The porosity is given by the ratio between the fluid section and the total section of the experiment: $\phi = 0.594$. The value of the hydraulic diameter is computed from the geometry $D_h = 0.01028$ m, and the value of the longitudinal friction coefficient C_f is given by empirical correlations [17] for this rod bundle geometry. The macroscopic turbulence model equations proposed here is solved. Symmetry conditions are used for the upper and lower boundaries, and for the lateral boundaries. In the normal and spanwise directions, only one node is taken, since the problem reduces to a one-dimensional problem. In the streamwise direction we take 50 nodes to ensure a sufficient resolution. The computation is started at a distance of $x/D_h = 2$ downstream the grid where is situated the first experimental measurement point. The results of $\langle k\rangle_f$ and an estimation of $\langle \epsilon\rangle_f$ obtained from the experiment are used as inlet conditions. The estimation of $\langle \epsilon\rangle_f$ is obtained using Eq. (16) and the two first experimental values of $\langle k\rangle_f$. The value for c_p is obtained from the experimental measurements far away from the grid, in the region where the flow is established: $c_p = 0.0368$. This is a value very close to the one obtain for flows inside pipes. Since we do not have access to the dissipation rate, the value of y^+_{lim} is unknown. We choose the value which gives the best result: $y^+_{lim} = 16$, which is still in the estimated range [5–30]. Fig. 9 shows the decay predicted by the present macroscopic model along with the intrinsically averaged values of the experiment. Results are presented in a dimensionless form. $\langle k\rangle_f$ at the equilibrium is the reference value for the macroscopic turbulent kinetic energy, and D_h is the reference for the distance. The good agreement between the two sets of results gives support to our model.

The value of y^+_{lim} that gives the right solution for this study is greater than the value recommended for pipe or channel flows. It could be explained either by a stronger direct dissipation in tube bundles than in pipes, or by the strong mean velocity gradients induced by the grid inside the core flow which create a strong direct dissipation that is not taken into account by our model (with our model, we only evaluate the dissipation due to the walls). We do not know which phenomena is predominant since we do not have any estimation of the dissipation rate inside the experiment. A microscopic calculation of the experiment could be undertaken to get an insight, however it is not in the scope of this article.

Note: With these two test cases, it is impossible to check the assumption made for the macroscopic turbulent viscosity (15). Indeed, the macroscopic turbulent viscosity only appears in diffusion terms in the macroscopic set of Eqs. (14), (16) and (17), and these diffusion terms are always negligible in the selected test cases. Another test case should be chosen to check this assumption if the user wants to use the model when macroscopic diffusion is not negligible. The same remark can be made for the macroscopic turbulent Prandtl numbers appearing in Eqs. (16) and (17).

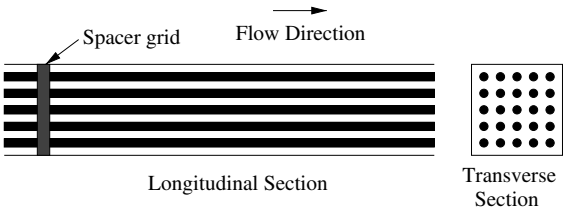

Fig. 8. Geometry of the AGATE experiment.

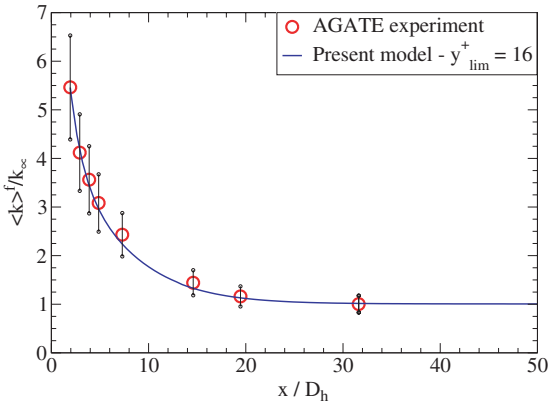

Fig. 9. Decay of turbulent kinetic energy.

6. Conclusion

In the literature, a macroscopic two-equation turbulence model obtained applying the volume-averaging theory to the microscopic two-equation turbulence model is proposed. The additional turbulent source terms appearing as an output of the averaging process are production terms of turbulent kinetic energy and its dissipation rate, and give account of the effect of the solids inside the flow, in the integration domain. These additional turbulent source terms have been modeled using the assumption that correlations obtained at equilibrium (uniform flows) are still valid out of equilibrium. The form of the dissipation turbulent source term has also been discussed. This study focus on longitudinal flows in arrays of channels, pipes or needles. The correlations have been established for longitudinal flows using the kinetic energy balance, an estimation of the direct viscous dissipation and by introducing an ad hoc length scale. The two unknown constants of this model have been determined using both numerical and experimental results. Thus, the model is valid for uniform fully developed flows at equilibrium in pipes and channels. The model has been also successfully evaluated against two sets of data of decreasing turbulence: a channel flow (3D calculation) and a rod bundle flow (experiment). Further investigation is needed to find out if the macroscopic models developed for transverse flows (square and circular rods) and longitudinal flows (channel, pipe and rod bundle flows) can be gathered in a unified model that could deal with any kind of porous media morphology.

References

[1] G. Alvarez, P.E. Bournet, D. Flick, Two dimensional simulation of turbulent flow and transfer through stacked spheres, Int. J. Heat Mass Transfer 46 (2003) 2459–2469.

[2] B.V. Antohe, J.L. Lage, A general two-equation macroscopic turbulence model for incompressible flow in porous media, Int. J. Heat Mass Transfer 40 (1997) 3013–3024.

[3] J. Bear, Dynamics of Fluids in Porous Media, American Elsevier, New York, 1972.

[4] C. Calvin, O. Cueto, P. Emonot, An object-oriented approach to the design of fluid mechanics software, Math. Modell. Numer. Anal. 36 (5) (2002) 907–921.

[5] Y.S. Chen, S.W. Kim, Computation of turbulent flows using an extended k–ϵ turbulence closure model, NASA CR-179204, 1987.

[6] K. Chung, K.-S. Lee, W.-S. Kim, Modified macroscopic turbulence modeling for the tube with channel geometry in porous media, Numer. Heat Transfer, Part A 43 (2003) 659–668.

[7] G. Comte-Bellot, Ecoulement turbulent entre deux parois parallèles, Publications Scientifiques et Techniques du Ministère de l'Air no. 419, 1965.

[8] H.P.G. Darcy, Les fontaines publiques de la ville de Dijon, Victor Dalmont, Paris, 1856.

[9] R.B. Dean, Reynolds number dependence of skin friction and other bulk flow variables in two-dimensional rectangular duct flow, J. Fluids Eng. 100 (1978) 215–223.

[10] J.G.M. Eggels, F. Unger, M.H. Weiss, J. Westerweel, R.J. Adrian, R. Friedrich, F.T.M. Nieuwstadt, Fully developed turbulent pipe flow: a comparison between direct numerical simulation and experiment, J. Fluids Mech. 268 (1994) 175–209.

[11] P. Emonot, Méthodes de Volumes Elements Finis: Application aux équations de Navier–Stokes et résultats de convergence, Ph.D. thesis, Université Claude Bernard—Lyon I, 1992.

[12] F. Falk, A. Memponteil, Détermination d'un champ de vitesses 3D en géométrie complexe par vélocimétrie laser 2d, in: 6ème Congrès francophone de Vélocimétrie laser, Saint Louis, France, 22–25 September 1998.

[13] D. Getachew, W.J. Minkowycz, J.L. Lage, A modified form of the k–ϵ model for turbulent flows of an incompressible fluid in porous media, Int. J. Heat Mass Transfer 43 (2000) 2909–2915.

[14] B. Guo, A. Yu, B. Wright, P. Zulli, Comparison of several turbulence models applied to the simulation of gas flow in a packed bed, in: Third Int. Conf. on CFD in the Minerals and Process Industries, CSIRO, Melbourne, Australia, 2003, pp. 509–514.

[15] C.V. Hirt, B.D. Nichols, N.C. Romero, Sola—a numerical solution algorithm for transient flow, Los Alamos National Laboratory, Report LA-5852, 1975.

[16] I.E. Idel'cik, Memento des pertes de charge, Direction des etudes et recherches d'EDF, 1969.

[17] S. Kakac, R.K. Shah, W. Aung, Handbook of Single-Phase Convective Heat Transfer, John Wiley & Sons, New York, 1987.

[18] F. Kuwahara, Y. Kameyama, S. Yamashita, A. Nakayama, Numerical modeling of turbulent flow in porous media using a spatially periodic array, J. Porous Media 1 (1) (1998) 47–55.

[19] F. Kuwahara, A. Nakayama, H. Koyama, A numerical study of thermal dispersion in porous media, J. Heat Transfer 118 (1996) 756–761.

[20] F. Kuwahara, M. Shirota, A. Nakayama, A numerical study of interfacial convective heat transfer coefficient in two-energy equation model for convection in porous media, Int. J. Heat Mass Transfer 44 (2001) 1153–1159.

[21] J.L. Lage, The fundamental theory of flow through permeable porous media from Darcy to turbulence, in: D.B. Ingham, I. Pop (Eds.), Transport Phenomena in Porous Media, 1998.

[22] B.E. Launder, D.B. Spalding, Mathematical Models of Turbulence, Academic Press, London, 1972.

[23] T. Mazuoka, Y. Takatsu, Turbulence model for flow trough porous media, Int. J. Heat Mass Transfer 39 (1996) 2803–2809.

[24] R.D. Moser, J. Kim, N.N. Mansour, Direct numerical simulation of channel flow up to $Re_\tau = 590$, Phys. Fluids 4 (11) (1999) 943–945.

[25] A. Nakayama, F. Kuwahara, A macroscopic turbulence model for flow in a porous medium, J. Fluids Eng. 121 (1999) 427–433.

[26] A. Nakayama, F. Kuwahara, T. Hayashi, Numerical modelling for the three-dimensional heat and fluid flow through a bank of cylinders in yaw, J. Fluid Mech. 498 (2004) 139–159.

[27] M.H.J. Pedras, M.J.S. de Lemos, On the definition of turbulent kinetic energy for flow in porous media, Int. Commun. Heat Mass Transfer 27 (2) (2000) 211–220.

[28] M.H.J. Pedras, M.J.S. de Lemos, Macroscopic turbulence modeling for incompressible flow through undeformable porous media, Int. J. Heat Mass Transfer 44 (2001) 1081–1093.

[29] M.H.J. Pedras, M.J.S. de Lemos, On the mathematical description and simulation of turbulent flow in a porous medium formed by an array of elliptic rods, J. Fluids Eng. 123 (2001) 941–947.

[30] M.H.J. Pedras, M.J.S. de Lemos, Simulation of turbulent flow in porous media using a spatially periodic array and a low Reynolds two-equation closure, Numer. Heat Transfer, Part A 39 (2001) 35–59.

[31] A.E. Perry, S.M. Henbest, M.S. Chong, A theoretical and experimental study of wall turbulence, J. Fluid Mech. 165 (1986) 163–199.

[32] J.C. Slattery, Momentum, Energy and Mass Transfer in Continua, McGraw-Hill, New York, 1972.

[33] K. Vafai, C.L. Tien, Boundary and inertia effects on flow and heat transfer in porous media, Int. J. Heat Mass Transfer 24 (1981) 195–203.

[34] S. Whitaker, Advances in theory of fluid motion in porous media, Ind. Eng. Chem. 61 (1969) 14–28.

[35] S. Whitaker, Flow in porous media I: A theoretical derivation of Darcy's law, Transp. Porous Media 1 (1986) 3–25.